ADVANCED MATERIALS

DOI: 10.1002/adma.200502569

Nanoscale Surface Morphology and Rectifying Behavior of a Bulk Single-Crystal Organic Semiconductor**

By *Etienne Menard*, *Alexandr Marchenko*, *Vitaly Podzorov*, *Michael E. Gershenson*, *Denis Fichou*,* and *John A. Rogers**

Single-crystal organic semiconductors represent perfect systems not only for studying basic science associated with transport of polaronic charge carriers but also for investigating the upper limits of mobilities in thin-film organic devices for flexible displays and other emerging electronic applications. The field-effect transistor provides an important tool to explore the transport of field-induced charge carriers at the surface of organic semiconductors.[1] Special care, however, must be taken during the device fabrication to avoid degradation of the critical interface between the semiconductor and the dielectric.[2,3] High material purity, excellent crystalline quality, and nanoscale morphological smoothness are among the characteristics of this interface that are crucial to obtaining high-performance devices[4,5] and test structures for studies of intrinsic phenomena.

Local surface measurements of organic semiconductors at the active interfaces of conventional transistors are difficult to perform, if not impossible, due to the inaccessibility of the semiconductor/gate dielectric interface by many classes of useful probes.[6–9] A new method for building transistors on the pristine surfaces of bulk single crystals uses free-space dielectrics (i.e., vacuum or air) to eliminate completely any contact or processing of the active surface of the semiconductor.[10] This technique, which provides a reversible ability to assemble and dissemble the devices repetitively, recently enabled observation of intrinsic transport and transport anisotropy in rubrene.[10,11] Other groups, using different techniques, have observed similarly high mobilities and orientational anisotropy.[3,12–14] Unlike organic monolayers and thin films for which several scanning tunneling microscopy (STM) studies have been reported in the past,[6,15–17] bulk organic crystals with thicknesses ranging from a few micrometers up to millimeters cannot be imaged by STM because of their inherent high electrical resistivity. We found that the only STM study of a bulk organic crystal was reported in 1988 by Sleator and Tycko on tetrathiafulvalene–tetracyanoquinodimethane (TTF–TCNQ),[18] later developed by Wang et al.[19]. These authors were able to image the surface of TTF–TCNQ crystals down to molecular resolution. However, being a charge-transfer salt, TTF–TCNQ possesses a metallic conductivity and therefore is much different from an organic semiconductor in terms of charge transport. Furthermore, this early study is limited to surface morphology and does not report on local transport properties by scanning tunneling spectroscopy (STS).

In this paper, we report on a nanoscale investigation of the critical interface between bulk single crystals of rubrene and air (i.e., the gate dielectric in the above-mentioned transistors) by means of STM and current–voltage (*I–V*) spectroscopy. In spite of dimensions as large as a few millimeters, the high conductivity and structural quality of undoped rubrene single crystals allows the imaging of their surfaces down to molecular resolution. STM images, combined with atomic force microscopy (AFM) and X-ray diffraction (XRD), reveal directly the position and orientation of individual molecules in the *a–b* plane which is used for fabrication of high-mobility field-effect transistors. Besides, local *I–V* curves recorded by STS in the dark and under light on the rubrene single crystals indicate a strongly rectifying p-type behavior. These nearly ideal *I–V* characteristics observed at the nanoscale are also observed on point-contact diodes on top of the rubrene crystals. Such remarkable transport properties indicate that the rubrene crystals are free of the surface transport channels that are commonly observed in inorganic semiconductors owing to dangling bonds.

High-quality single crystals of rubrene were grown by physical-vapor transport in hydrogen.[1] Figure 1A shows an optical image of a typical crystal with an elongated hexagonal plate shape and dimensions of 4 mm × 1.5 mm × 0.5 mm. The orientation of the crystal axis was determined by XRD using Cu Kα radiation. Figure 1C shows the 2θ X-ray (45 kV, 40 mA, 2 s per angle step) intensity data collected on this crystal. The polar plots show that, as typically observed for crystals belonging to the orthorhombic pyramidal point group,[20] the *c*-axis is normal to the top surface (slow-growing face) and the *b*-axis

[*] Prof. D. Fichou, Dr. E. Menard, Dr. A. Marchenko
CEA-Saclay, LRC Nanostructures et Semi-Conducteurs Organiques
CNRS-CEA-UPMC, SPCSI/DRECAM
91191 Gif-sur-Yvette (France)
E-mail: fichou@drecam.cea.fr
Prof. J. A. Rogers, Dr. E. Menard
Departments of Materials Science and Engineering,
Electrical and Computer Engineering, and Chemistry
Beckman Institute
and Frederick Seitz Materials Research Laboratory
University of Illinois at Urbana/Champaign
Urbana, IL 61801 (USA)
E-mail: jrogers@uiuc.edu
Dr. V. Podzorov, Prof. M. E. Gershenson
Department of Physics and Astronomy, Rutgers University
Piscataway, NJ 08854 (USA)

[**] This work was supported by the NSF grants DMR-0405208 and ECS-0437932. Supporting Information is available online from Wiley InterScience or from the author.

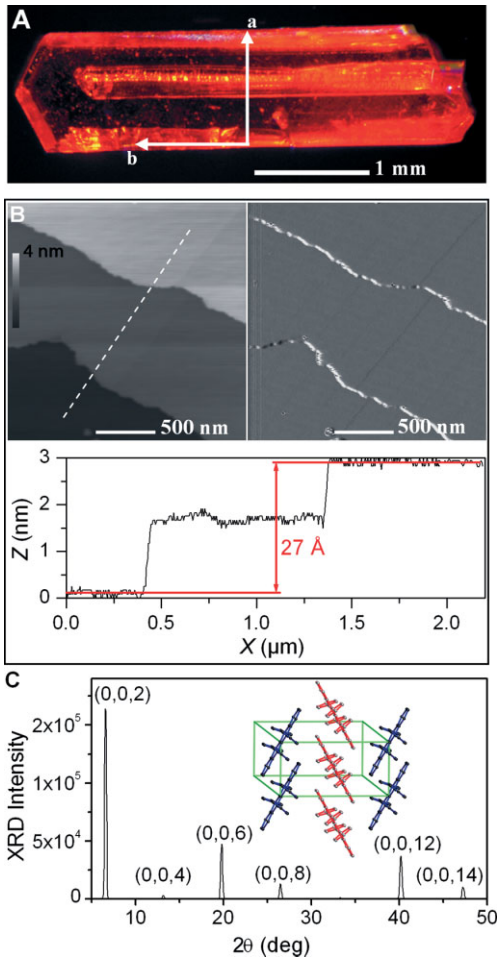

Figure 1. A) Optical microscopy image of a rubrene single crystal with dimensions 4 mm × 1 mm × 0.5 mm. The directions of the *a* and *b* crystal axes are determined by XRD. B) AFM topography (left) and phase (right) images of the surface of the sample. The bottom graph shows molecular steps with 27 ± 0.5 Å heights. C) XRD 2θ plot of the sample with an inset that shows schematically the molecular organization of the rubrene molecules in the crystal *a*–*b* plane. The extracted orthorhombic cell lattice dimensions are $a = 14.49$ Å, $b = 7.21$ Å, $c = 26.92$ Å.

is parallel to the long side of the crystal. The crystal lattice values determined from these measurements are similar to those published in the literature: $a = 14.49$ Å, $b = 7.21$ Å, $c = 26.92$ Å.[21,2] The vertical distance measured by AFM between three terraces (see Fig. 1B, bottom inset) is in good agreement with the *c*-axis crystal-lattice parameter. This result confirms that a unit orthorhombic cell in rubrene consists of two nonequivalent *a*–*b* molecular planes (the space group *Aea*2, No. 41, former *Aba*2); the distance ca. 27 Å in Figure 1b corresponds to the spacing between identical planes in two adjacent unit cells.[23] AFM images (Fig. 1B) of the surface show flat terraces (as revealed by the phase image) separated by monomolecular steps. Images recorded at various locations indicate that the terrace plains are parallel to each other, suggesting that the samples are single-crystalline.

STM enables the direct examination of the molecular packing at the organic surface, and the transport properties of the semiconductor/gate dielectric interface in our transistors.[10] For STM and STS measurements, the sample was mounted onto a metal plate using silver paint and left overnight for the paint to dry. STM imaging and STS were performed with a PicoScan STM ("Molecular Imaging/Agilent Technology") equipped with a low-current scanning head. The Pt–Ir (80:20) tip was mechanically cut from a commercial wire of 0.25 mm diameter. The STM images were recorded in both "current" and "constant height" modes. Molecular-scale images were recorded at negative tip polarities between –1 and –2 V. At positive voltages, virtually no tunneling current was recorded for reasons described below.

Figure 2A shows a typical STM image of the rubrene surface. Two flat terraces separated by an approximately 2 nm high step are visible in the left and right parts of the image

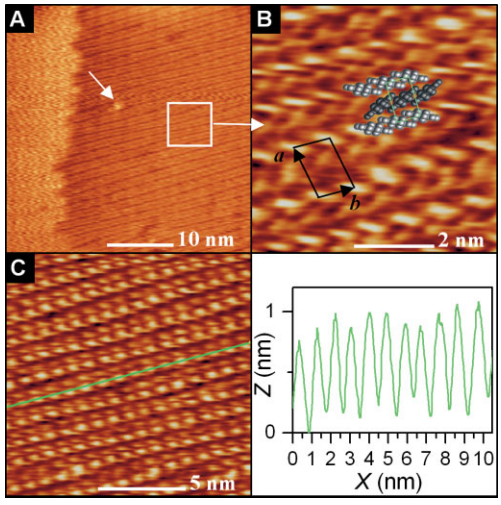

Figure 2. STM images of the rubrene surface. A) Typical large-scale STM image of the rubrene crystal surface in the constant-current mode ($U_t = -1.065$ V, $I_t = 29$ pA). B) A smaller-scale image ($U_t = -1.138$ V, $I_t = 29$ pA) reveals the herringbone organization of the rubrene molecules in the *a*–*b* plane. C) Larger-scale image and cross-sectional profile along a single row of molecules in the *b*-axis direction of the crystal.

(AFM measurements provide more accurate step-height measurements). The large terrace in the right part reveals parallel rows extending along a preferential crystallographic direction. The average Z-corrugation of the rows is estimated to be about 1.5 Å. The detailed shape of the step between the terraces can change slightly during scanning, which suggests tip-induced detachment of molecules from the step edge, as described below. Some detached molecules appear on top of the terrace (shown by a white arrow in Fig. 2A). This tip-induced detachment of the molecules leads to instability in the tunneling gap and the loss of resolution in the left part of the image in Figure 2A. In the course of the STM scan, we observed an interesting tip-induced layer-by-layer desorption process of

ADVANCED MATERIALS

the rubrene crystal surface. Details concerning this unusual phenomenon are given in the online Supporting Information (Figs. S1 and S2). Several topographic images acquired at different areas indicate that the orientation of molecular rows is spatially uniform. Figure 2B is a high-resolution image of the main domain of Figure 2A showing individual molecules in a herringbone packing. The distance between the repeated double-row features is approximately 14 Å, while that between molecules within a row is approximately 7 Å. Comparison with the lattice parameters obtained by XRD confirmed that we are imaging the *a*–*b* plane of the crystal. The parallelogram drawn in Figure 2B shows the unit cell in the *a*–*b* plane of the rubrene crystal. Figure 2C shows an intermediate scale image together with a cross-sectional profile along a single row of molecules in the direction of the *b*-axis. These observations are important because they indicate an atomically clean interface and single-crystal molecular organization at the active interface of transistors that use the as-grown surfaces of rubrene crystals as the semiconductor and air as the dielectric.

Figure 3A shows a set of six *I*–*V* STS traces recorded by positioning the tip at the apex on six different places of a molecularly flat terrace, such as the one shown in Figure 2C. The six curves have identical profiles regardless of the recording place which is quite unusual for STS measurements carried out in ambient conditions. In these STS measurements the feedback loop of the STM is disabled, so that after the initial regulation setpoint ($I_t = 10$ pA, $U_t = -1.1$ V) and thus the tip height has been fixed, the subsequent voltage variations are not followed by a vertical movement of the tip. Rather, the tip remains at the initial height and the change in current resulting from the change in voltage is recorded. For negative tip voltages, a steep and almost linear increase of the tunnel current occurs beyond a threshold voltage of –0.3 V. At positive polarity the measured current is close to zero. The turn-on voltages of the diodes are in good agreement with measurements made on a bulk point-contact Schottky diode (Fig. 4A).[24] This result suggests that the STM tip comes into close contact with the rubrene during the scan.

The rubrene point-contact Schottky diodes (Fig. 4A) also shows extremely good current-blocking behavior up to reverse voltage biases of approximately 20 V. The nearly zero (< 0.35 pA V^{-1}) ohmic "leakage" current in the reverse bias regime ($U_t > 0$) indicates the absence of a surface transport

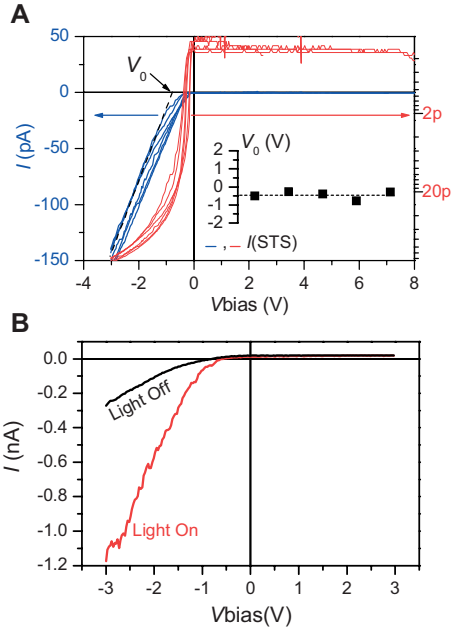

Figure 3. STS on the rubrene bulk single-crystal surface. A) *I*–*V* tunneling spectra of the tunnel diode presented on a linear (left) and logarithmic (right) axis showing the perfectly rectifying behavior of the p-type rubrene semiconductor. The inset plot shows the extracted turn-on voltages from the tunneling spectra. B) *I*–*V* tunneling spectra recorded in the dark and under white-light excitation at a different location on the rubrene crystal.

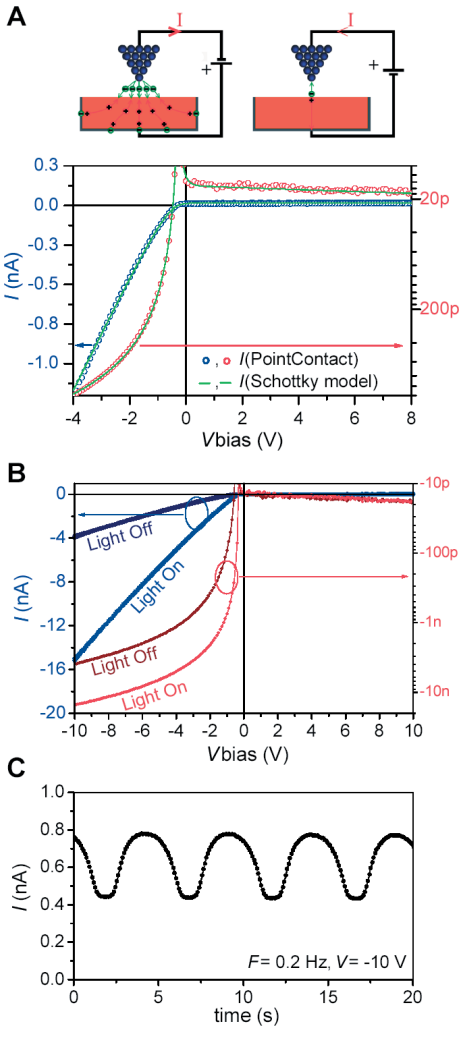

Figure 4. Rubrene bulk crystal point-contact diode. A) *I*–*V* characteristic of a rubrene point-contact diode (dots) fitted with the Schottky model (line). The top scheme illustrates the carrier injection mechanism at the tip and bottom electrodes of the point-contact diode. B) *I*–*V* characteristics of the device under white-light excitation. C) Time dependence of the forward-current amplitude upon exposure to a white light-emitting diode electronically modulated with a 0.2 Hz sinus wave.

channel related to dangling bonds.[25] This remarkable behavior is much different from that observed in silicon point-contact diodes, for example. The extremely low current recorded under positive biases derives from the high quality of the rubrene crystals and the intrinsic absence of dangling bonds on the surface of molecular solids. This type of behavior has not been previously examined directly, although it is consistent with the extremely sharp normalized subthreshold swing for rubrene field-effect transistors that use air as a gate dielectric.[10] In the forward regime ($U<0$), the current of the diodes is linearly limited by the very high resistivity of the rubrene crystal. Since the quantity of injected charges is not sufficient (low voltage biases applied on a thick crystal) to enter into the space-charge-limited current regime, the *I–V* characteristic is expected to be linear (ohmic regime supported by thermal carrier generation).[26] A bulk conductivity of approximately 0.4 nS is extracted from the point-contact diode after fitting the *I–V* characteristic with a standard Schottky exponential model and assuming a thermionic current emission, a serial resistance R_s, a parallel leakage resistance R_p and a reverse current I_r (Eq. 1).[27]

$$I = I_S\left[e^{\frac{V-R_S\cdot I}{n\cdot k\cdot T}} - 1\right] + \frac{V - R_s\cdot I}{R_p} - I_r \qquad (1)$$

with $I_s = 2.1$ pA, $n = 5.5$, $R_s = 2.65$ GΩ, $R_p = 3$ TΩ, and $I_r = 13$ pA (k: the Boltzmann constant; T: temperature). These results indicate the p-type rectifying behavior of the rubrene single crystal where positive carriers are injected (from the bottom contact) as schematically illustrated in the top scheme of Figure 4A. Only positive carriers transit through the bulk while electrons, which possess much lower mobilities, are probably trapped.[28] We measured the concentration of deep traps (N_{tr}) in our rubrene crystals using free-space field-effect transistor devices and found it to be of the order of $N_{tr} = 0.7\times10^{10}$ cm^2 at 300 K. The hole mobilities along the *a*- and *b*-axes are of the order of $\mu_h = 15$–20 cm^2 V^{-1} s^{-1}, as measured directly on pristine surfaces of samples such as those examined here by STM and point-contact diodes. As expected from the above interpretation, point-contact diodes fabricated using low-work-function metal electrodes such as Ca also show p-type rectifying behavior with a similar conduction mechanism involving primarily holes. Additional experiments with other metals would help to support such a conclusion.

In order to explore whether the p-type rectifying behavior of rubrene crystals is a property inherent to these samples, we recorded the STS and point-contact diode *I–V* characteristics under white-light illumination (see Figs. 3B and 4B). In both types of systems for negative tip voltages (passing side) the current flowing through the crystal increases by a factor of approximately four, as compared to the dark. The light induces both electrons and holes (and resulting excitons), but for positive biases (blocking side), the current remains extremely weak and is unaffected by light excitation (see the logarithm scale on the right axis in Fig. 4B). Intense light may induce thermal effects, such as tip dilatation for example, thus resulting in a noticeable change in the *I–V* characteristics. Here, thermal effects are excluded because we use an optic fiber delivering white light with intensities of the order of 10–15 mW cm^{-2}. STS reveals rectifying behavior in the transport, consistent with point-contact diode measurements using several different metals. The observation that the conduction mechanism remains strictly unipolar even under illumination suggests that the p-type rectifying behavior arises from a sample property (e.g., the presence of traps for electrons) rather than preferential hole injection dictated by the nature of the contacts. Finally, Figure 4C shows that it is possible to modulate the photocurrent on the passing side with a frequency of 0.2 Hz, indicating good stability of the metal–rubrene crystal junction under light exposure.[29]

In conclusion, high-resolution STM images and nanoscale *I–V* characteristics of rubrene single crystals with dimensions of several millimeters have been recorded. The periodic 2D organization of individual molecules of rubrene, an organic semiconductor with potential applications in electronics, have been observed on the *a–b* plane of a bulk crystal where they form a highly ordered step and terrace surface. With the exception of of TTF–TCNQ, an organic charge-transfer salt with metallic conductivity, surface imaging of bulk crystal organic semiconductors has always failed because of their low dark conductivity. Another prominent feature is that STS reveals the nearly perfect rectifying behavior of the rubrene crystals. While intense currents flow at negative tip voltages, almost no current can be recorded at positive tip voltages up to several volts. This is typical of a unipolar p-type semiconductor. Furthermore, when exposed to white light, rubrene bulk crystals generate intense photocurrents under negative tip voltage while no increase of the conductivity is observed on the blocking side. On the whole, our data directly reveal the nanoscale morphology and electrical properties of the active interfaces of field-effect transistors fabricated with these materials. Finally, beyond the scope of this semiconductor analysis, the surface morphology and transport properties of bulk rubrene crystals suggest that they could be used as novel STM substrates. The presence of large molecularly flat terraces on the crystal *a–b* plane combined with good conductivity opens the possibility to investigate adsorption and self-assembly of various organic molecules and other nanometer-sized objects.

Received: November 30, 2005
Final version: March 8, 2006
Published online: May 18, 2006

[1] R. W. I. de Boer, M. E. Gershenson, A. F. Morpurgo, V. Podzorov, *Phys. Status Solidi A* **2004**, *201*, 1302.
[2] H. E. Katz, Z. Bao, *J. Phys. Chem. B* **2000**, *104*, 671.
[3] C. Goldmann, S. Hass, C. Krellner, K. P. Pernstich, D. J. Gundlach, B. Batlogg, *J. Appl. Phys.* **2004**, *96*, 2080.
[4] V. Podzorov, S. E. Sysoev, E. Loginova, V. M. Pudalov, M. E. Gershenson, *Appl. Phys. Lett.* **2003**, *83*, 3504.
[5] V. C. Sundar, J. Zaumseil, V. Podzorov, E. Menard, R. L. Willett, T. Someya, M. E. Gershenson, J. A. Rogers, *Science* **2004**, *303*, 1644.

ADVANCED MATERIALS

[6] D. Fichou, F. Charra, A. O. Gusev, *Adv. Mater.* **2001**, *13*, 555.
[7] D. Knipp, R. A. Street, A. Volkel, J. Ho, *J. Appl. Phys.* **2003**, *93*, 347.
[8] R. J. Chesterfield, J. C. McKeen, C. R. Newman, C. D. Frisbie, P. C. Ewbank, K. R. Mann, L. L. Miller, *J. Appl. Phys.* **2004**, *95*, 6396.
[9] W. A. Schoonveld, J. Wildeman, D. Fichou, P. A. Bobbert, B. J. van Wees, T. M. Klapwijk, *Nature* **2000**, *404*, 977.
[10] E. Menard, V. Podzorov, S.-H. Hur, A. Gaur, M. E. Gerschenson, J. A. Rogers, *Adv. Mater.* **2004**, *16*, 2097.
[11] V. Podzorov, E. Menard, A. Borisson, V. Kiryukhin, J. A. Rogers, M. E. Gershenson, *Phys. Rev. Lett.* **2004**, *93*, 086 602.
[12] R. Zeis, C. Besnard, T. Siegrist, C. Schlockermann, X. L. Chi, C. Kloc, *Chem. Mater.* **2006**, *18*, 244.
[13] Z. L. Rang, M. I. Nathan, P. P. Ruden, V. Podzorov, M. E. Gershenson, C. R. Newman, C. D. Frisbie, *Appl. Phys. Lett.* **2005**, *86*, 123 501.
[14] R. W. I. de Boer, N. N. Iosad, A. F. Stassen, T. M. Klapwijk, A. F. Morpurgo, *Appl. Phys. Lett.* **2005**, *86*, 032 103.
[15] J. K. Gimzewski, J. H. Coombs, R. Möller, R. R. Schlittler, in *Molecular Electronics-Science and Technology* (Ed: A. Aviram), Engineering Foundation, New York **1990**, pp. 87–94.
[16] S. F. Alvarado, L. Rossi, P. Müller, W. Riess, *Synth. Met.* **2001**, *122*, 73.
[17] M. M. S. Abdel-Mottaleb, E. Gomar-Nadal, S. De Feyter, M. Zdanowska, J. Veciana, C. Rovira, D. B. Amabilino, F. C. De Schryver, *Nano Lett.* **2003**, *3*, 1375.
[18] T. Sleator, R. Tycko, *Phys. Rev. Lett.* **1988**, *60*, 1418.
[19] Z. Z. Wang, J. C. Girard, C. Pasquier, D. Jérome, K. Bechgaard, *Phys. Rev. B* **2003**, *67*, 121 401.
[20] C. Kloc, P. G. Simpkins, T. Siegrist, R. A. Laudise, *J. Cryst. Growth* **1997**, *182*, 416.
[21] D. McLachlan, *X-Ray Crystal Structure*, McGraw-Hill, New York **1957**.
[22] D. E. Henn, W. G. Williams, D. J. Gibbons, *J. Appl. Crystallogr.* **1971**, *4*, 256.
[23] T. Hahn, *International Tables for Crystallography: Brief Teaching Edition of Space Group Symmetry*, Kluwer, Dordrecht, The Netherlands **2001**.
[24] The point-contact diode was made using a 12 μm tip diameter tungsten carbide probe tip from Signatone.
[25] P. Avouris, I. W. Lyo, Y. Hasegawa, *IBM J. Res. Dev.* **1995**, *39*, 603.
[26] Onset of the trap-filled limit (TFL) current $U_{TFL} = Nt\varepsilon\varepsilon_0/(eL^2)$. See: M. Pope, C. E. Swenberg, *Electronic Processes in Organic Crystals and Polymers*, Oxford Science Publications, New York **1999**, p. 387.
[27] S. M. Sze, *Semiconductor Devices, Physics and Technology*, Wiley, New York **2002**.
[28] W. G. Williams, *Faraday Discuss.* **1991**, *51*, 61.
[29] V. Podzorov, V. M. Pudalov, M. E. Gershenson, *Appl. Phys. Lett.* **2004**, *85*, 6039.